The Effect of East African Topography on Flow Driven by Zonally Symmetric Forcing

JAN PAEGLE AND J. E. GEISLER

Department of Meteorology, University of Utah, Salt Lake City, UT 84112

(Manuscript received 29 May 1984, in final form 28 February 1986)

ABSTRACT

The low-level circulation in summer over the western Indian Ocean is characterized by southeast trades that are channeled near the African coast into a concentrated southerly flow across the equator and thence northeastward into the southwest monsoon over the Arabian Sea. It is widely accepted that deflection by the East African highlands is responsible for this flow configuration. Existing theoretical models, to a greater or lesser extent, build in this deflection by imposing a western boundary extending all the way to the top of the fluid or by prescribing longitudinally dependent sources and sinks for driving the flow.

The purpose of this study is to determine what flow configuration occurs when these constraints are removed. For this we use zonally symmetric forcing to drive a planetary boundary layer model formulated in a terrain-following coordinate system that permits fluid to flow over, as well as along, a topographic barrier. The results support the conclusion that East African topography alone can channel incident flow into a pattern with most of the observed features. An analysis of the diurnal oscillation in the model suggests a mechanism for the diurnal variation of low-level wind observed in northeastern Somalia.

1. Introduction

The prevailing interpretation of the East African jet (EAJ) is that it is a western boundary current. Like its ocean-basin counterparts, the EAJ has been analyzed with linear and nonlinear barotropic vorticity balance models. Thus, in the model of Anderson (1976), lateral friction at a vertical western boundary is the vorticity sink mechanism; Hart (1977) has formulated a model with bottom friction acting on a fluid bounded below by shelving topography. In the model of Hart (1977) the outer shear zone of the jet is an inertial boundary layer and the inner shear zone is produced by a combination of bottom friction and rapidly shelving topography. Krishnamurti et al. (1976) developed a nonlinear numerical model of the EAJ system having fine horizontal grid-point resolution and realistic East African topography. Bannon (1979a,b) generalized the model of Hart (1977) by carrying out numerical solutions of the nonlinear primitive equations in the presence of more realistic topography and a free-surface upper boundary. More recently, Bannon (1982) extended the domain of his model well to the north of the equator to model the separation of the EAJ (due to the topography of the African highlands and the local enhancement of the flow that is observed in the southwest monsoon over the Arabian Sea.

All of the above models were barotropic, with stratification included in the form of a reduced gravity that entered into the basic equatorial β-plane length and time scales. In all cases the motion field was driven by a prescribed mass source in the Southern Hemisphere together with a mass sink in the Northern Hemisphere. The presence of a western wall filling the vertical domain constitutes a strong constraint in that it forces all the fluid from the source to flow across the equator to reach the sink. Only the model of Bannon (1982) allowed for some spilling over the top of the topography and out through the western boundary of the model domain.

Krishnamurti et al. (1983) adopted a different approach to the modeling of the EAJ. Their model treats a fully stratified fluid and contains a detailed parameterization of subgrid scale processes acting in the planetary boundary layer. The model also employs realistic East African topography and very fine horizontal resolution. Motion is driven by a prescribed three-dimensional pressure field, based on observed data and characterized by considerable zonal asymmetry. The nonlinear primitive equations are marched forward in time with this driving pressure field until a steady state motion field is obtained.

The purpose of this paper is to present an analysis of some basic aspects of the EAJ using a detailed planetary boundary layer model formulated in terrain-following coordinates. From the standpoint of dynamics, the major difference between our study and that of Krishnamurti et al. (1983) is that we prescribe the pressure field only at the top of the model (at 3 km) and allow the pressure and motion field to develop below this level. There is also a difference in objectives. Krishnamurti et al. (1983) were interested in simulating the observed EAJ. In this study we produce several idealized examples of an EAJ and attempt to identify

what is responsible for the gross features in these examples.

In the model we present here, the forcing is independent of longitude. In the absence of topography the response consists of a purely zonal flow, antisymmetric with respect to the equator, plus a small northward drift in a near-surface boundary layer. Longitudinal structure that develops in this model has to be a consequence of longitudinal dependence on bottom topography, together with some contribution of longitudinally dependent low-level sensible heating, and not of prescribed longitudinally dependent monsoonal forcing. One goal of the study is to show that topography with a height equal to that of East Africa is sufficient to divert a substantial fraction of the model's zonal flow northward across the equator. We examine both the case of a straight north–south ledge and the case of realistic topography. In the former case, we present both nonlinear and quasi-linear solutions. The model incorporates the diurnal cycle of solar heating and, hence, diurnally varying static stability and vertical eddy diffusion. A second goal of the study is to present in the realistic topography case the diurnal cycle of the model wind field at a point in northeastern Somalia and to identify the dynamical factors in the model that are responsible for it.

2. The model

We consider an equatorial belt of stratified fluid situated on a sphere. The domain of the model is shown in Fig. 1, which also shows the topography of East Africa that we will use in the realistic-topography run described later. A filled circle denotes the point at which we subsequently examine the diurnal variation of the low-level wind field. The zero contour outlines the east coast of Africa and the island of Madagascar. The model itself, described fully in Paegle and McLawhorn (1983), uses a terrain-following coordinate system. In the present application, the fluid is assumed to have a constant depth of 3 km above the terrain; that is, the thickness of the fluid is spatially uniform and remains so throughout the time integration. A steady external forcing is imposed by prescribing at the upper boundary a pressure gradient that maintains there a geostrophically balanced zonal wind

$$u = U \tanh(\phi/\phi_0) \tag{1}$$

where $U = 10$ m s^{-1}, ϕ is latitude and $\phi_0 = 4°$. At lower levels the motion field and associated pressure field evolve in time to a quasi-steady state determined by the model dynamics and the topography.

The model equations are

$$\frac{Du}{Dt} - fv = -\frac{1}{\rho_s a \cos\phi}\frac{\partial p'}{\partial \lambda} - \frac{g\rho'}{\rho_s}\frac{1}{a\cos\phi}\frac{\partial Z}{\partial \lambda} T + \frac{\partial}{\partial z}\left(K_m \frac{\partial u}{\partial z}\right) + F_u, \tag{2}$$

$$\frac{Dv}{Dt} + fu = -\frac{1}{\rho_s a}\frac{\partial p'}{\partial \phi} - g\frac{\rho'}{\rho_s}\frac{1}{a}\frac{\partial Z}{\partial \phi} T + \frac{\partial}{\partial z}\left(K_m \frac{\partial v}{\partial z}\right) + F_v, \tag{3}$$

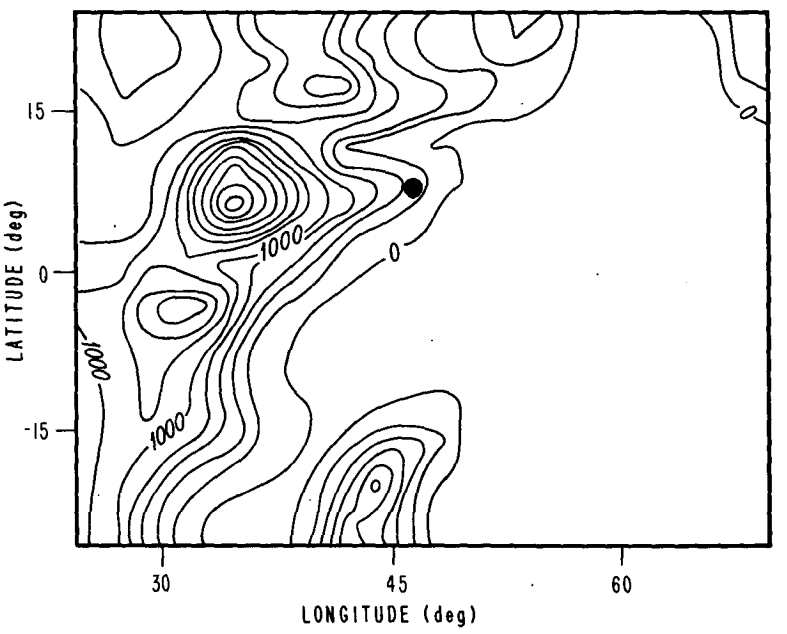

FIG. 1. Topography of East Africa and Madagascar used in the realistic topography run. Contour interval is 200 m. This figure also defines the horizontal domain of the model. A filled circle marks the location of the point where the diurnal oscillation of the wind is analyzed in section 3d.

$$0 = -\frac{\partial p'}{\partial z} - \rho' g, \tag{4}$$

$$\frac{1}{a\cos\phi}\frac{\partial u}{\partial \lambda} + \frac{\partial}{\partial \phi}(v\cos\phi) + \frac{\partial w}{\partial z} = 0, \tag{5}$$

$$\frac{D\theta}{Dt} = \frac{\partial}{\partial z}\left(K_H \frac{\partial \theta}{\partial z}\right) + \frac{Q}{c_p}\left(\frac{p_0}{p}\right)^{R/c} p + F_\theta. \tag{6}$$

Here D/Dt is the terrain-following convective derivative in spherical coordinates and $f = 2\Omega \sin\phi$. The terms $uv \tan\phi/a$ and $u^2 \tan\phi/a$ have been omitted from Eqs. (2) and (3), respectively, using the justification that the magnitude of these terms relative to the Coriolis terms is $u/(2\Omega a \cos\phi)$, which is of order 10^{-2} everywhere in the model domain.

In the foregoing equations z is a coordinate normal to the terrain. Because the terrain slope is everywhere less than 10^{-2}, this coordinate is essentially identical to altitude above the terrain, and we will refer to it as such. The variable Z_T is the terrain height. The basic-state temperature field in the model is a time-independent linear function of altitude above sea level. A subscript s denotes the associated basic-state density field. Primes are used to denote deviation of pressure and density from their basic-state values. The quantity θ in Eq. (6) is the sum of basic-state plus deviation potential temperature. The vertical eddy diffusion coefficient for momentum is given by

$$K_m = 0.2 b^{1/2} \ell$$

where ℓ is a mixing length and b is a turbulent kinetic energy which is calculated by a prognostic equation in the model. Details are given in Paegle and McLawhorn (1983). This determination of K_m is used from the surface to 500 m. Above this level K_m is assumed to decrease exponentially with an e-folding distance of 500 m. The vertical eddy diffusion coefficient for heat is specified to be $K_H = 1.35K_m$. The quantities denoted by a subscripted F in (2), (3) and (6) represent the presence in the model of horizontal eddy diffusion of the form first used in large-scale models by Smagorinsky (1963). The horizontal eddy diffusion coefficient is given by $K = 0.36|D|\delta^2$, where D is the deformation rate and δ is the horizontal grid-point spacing. The value of K is always $\leq 5 \times 10^5$ m^2 s^{-1}, a value which in this model produces diffusion of horizontal momentum and heat between two neighboring grid points on a time scale of one day.

The model contains a surface energy balance calculation in which sensible heat flux to the atmosphere is balanced by absorbed solar radiation, outgoing infrared, and a heat flux determined by solving the heat conduction equation in a subsurface soil layer. The soil type is dry sand. Over the entire domain, the albedo is taken as 0.4. In the present simulations we take the season to be late June and we incorporate the diurnal variation of solar radiation. For the duration of these model runs, the surface temperature of the ocean remains essentially constant at its initially prescribed value of 298 K, while the land-surface temperature varies diurnally in a reasonable manner.

Transfer of infrared radiation in the model follows the scheme of Zdunkowski et al. (1976). The only radiatively active gas is water vapor. It is initially distributed uniformly in the horizontal, decreasing linearly with height from a value of 14 gm kg^{-1} at sea level with a rate of decrease of 2.8 gm kg^{-1} km^{-1}. There is no evaporation or condensation in the model. The initial distribution of water vapor is subsequently somewhat altered by diffusion and advection, but with the constraint that the upper-boundary value remain at its initial value. Water vapor is carried in this model only to provide radiative cooling of the atmosphere.

The initial condition for the wind field is that it is in geostrophic balance above 200 m and decreases logarithmically to zero at a roughness height of 4 cm. The initial pressure field is determined from the prescribed pressure at the upper boundary, assuming a basic state temperature lapse rate of 6.5 K km^{-1}. The vertical temperature distribution in the region over water in the Southern Hemisphere is not much changed from this basic state value by processes in the model, so that the stratification of the flow incident on the coastline has $N^2 \approx 10^{-4}$ s^{-2}. Throughout the time integration, the flow is given by (1) at the upper boundary and is zero at the roughness height. The horizontal boundary conditions in the model are those of zero normal gradient for all prognostic variables.

The horizontal grid size in the model is 1.875° in both latitude and longitude. A stretched coordinate is employed in the vertical with very high resolution in the lowest 100 m. The locations of grid points in units of meters above topography are 0.04, 0.109, 0.296, 0.803, 2.18, 5.94, 16.1, 44, 119, 324, . . . (intervals of 205) . . . , 2987. The model time step is 10 min. In the case where the full model is used in the presence of realistic topography, a quasi-steady state is reached in 7 days. We also present results of some experiments with idealized topography and no model physics except a prescribed eddy diffusion. In these cases a quasi-steady state is reached in about 3 days.

3. Results

a. *No topography*

We examine first the zonally symmetric response when there is no topography and the forcing is given by (1). In this particular experiment (and the experiment described in section 3b), much of the model physics is omitted. Specifically, solar and infrared radiation is removed along with eddy diffusion of heat, and the momentum diffusion coefficient is prescribed to increase linearly with altitude to a value of 10 m^2 s^{-1} at 100 m and remain constant at higher levels. The

model is then integrated forward in time starting from the initial state described in section 2.

The resulting distributions of zonal and meridional winds are shown in Fig. 2a,b, respectively. As dictated by (1), the zonal wind is a maximum at the (open) side boundaries. Meridional flow passing in through the southern boundary, across the equator, and out the northern boundary is essentially confined to the lowest kilometer.

b. Ledge topography

In the first of two experiments with ledge topography, conditions are identical to those in the zonally symmetric experiment just described, with one exception: flat land of 1500 m elevation is imposed everywhere west of longitude 42.187°E. Figure 3 shows the horizontal wind field at four model levels 72 h after the start of the run. The gross features of the summer low-level wind field over the western Indian Ocean are reproduced. There are southeast trades in the Southern Hemisphere that converge into a cross-equatorial jet. In the Northern Hemisphere there has developed a southwest monsoon that is considerably stronger than the Southern Hemisphere trades. Beyond this time the pattern in Fig. 3 does not change, apart from the development of some small-amplitude wave structure in the southwest monsoon that can be interpreted as a downstream manifestation of the lee wave trough that is seen just east of the ledge in the Northern Hemisphere.

An equatorial cross section of the EAJ as it appears in this idealized-topography run is shown in Fig. 4. The ledge is displayed as a ramp extending between two horizontal grid points. Bottom friction and nonlinear advection terms are of comparable importance in the vorticity balance of the jet. Horizontal eddy diffusion in the model also influences the shape of this narrow jet. This horizontal eddy diffusion acts only to diffuse momentum on surfaces of a constant terrain-following coordinate and does not directly transport momentum to the boundary.

In the second ledge-topography experiment, the above run was repeated with the forcing reduced by an order of magnitude in order to obtain a solution where the dynamics are quasi-linear. Figure 5 shows a horizontal cross section at 529 m. A meridional jet runs parallel to the ledge over the entire domain of the model. The flow pattern is quite symmetric with respect to the equator. This figure is to be compared to the horizontal cross section at the same level shown in Fig. 3b. From this comparison we conclude that the important equatorially asymmetric features of separation of the jet from the ledge and formation of a strong southwest monsoon are effects of nonlinear dynamics. An equatorial cross section of this quasi-linear EAJ is shown in Fig. 6. Although the amplitude of the forcing function (1) has been reduced by a factor of 10, the jet maximum is only a factor of 4 smaller than the jet in Fig. 4. On its east side this jet is broader than the one in Fig. 4. On the west side the morphology of the two jets is very similar.

It was noted in the Introduction that a western boundary wall in a barotropic model simulation of the EAJ is a strong constraint because it forces all of the fluid introduced in a Southern Hemisphere source to move across the equator into a Northern Hemisphere sink. This strong constraint is not built into the present model, where fluid introduced in the Southern Hemisphere sink is free to flow westward up the ledge and out through the western boundary. It is possible in the present model to approximate this constraint by using a high ledge. Figure 7a shows the flow at a level 529

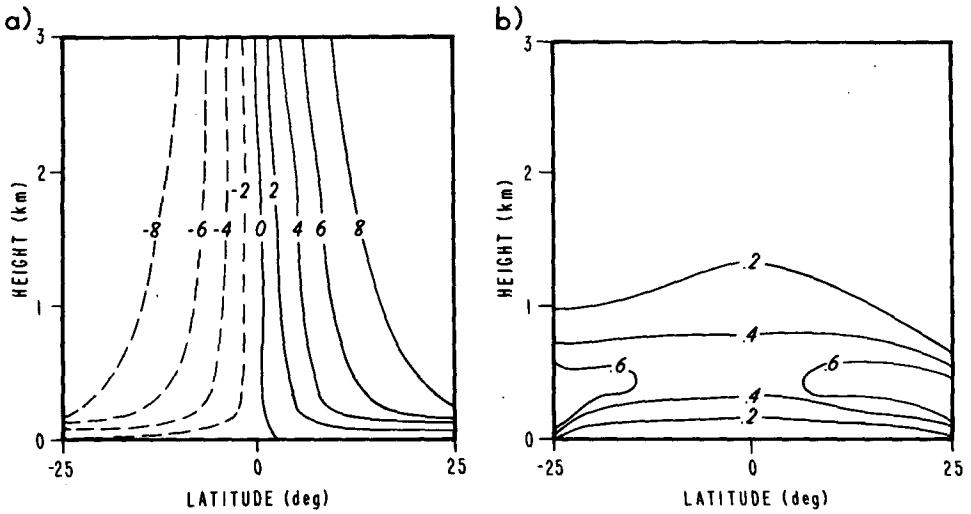

FIG. 2. The zonally symmetric response obtained when there is no topography in the model. Panels show (a) the zonal component of the wind and (b) the meridional component of the wind. Units are m s^{-1}.

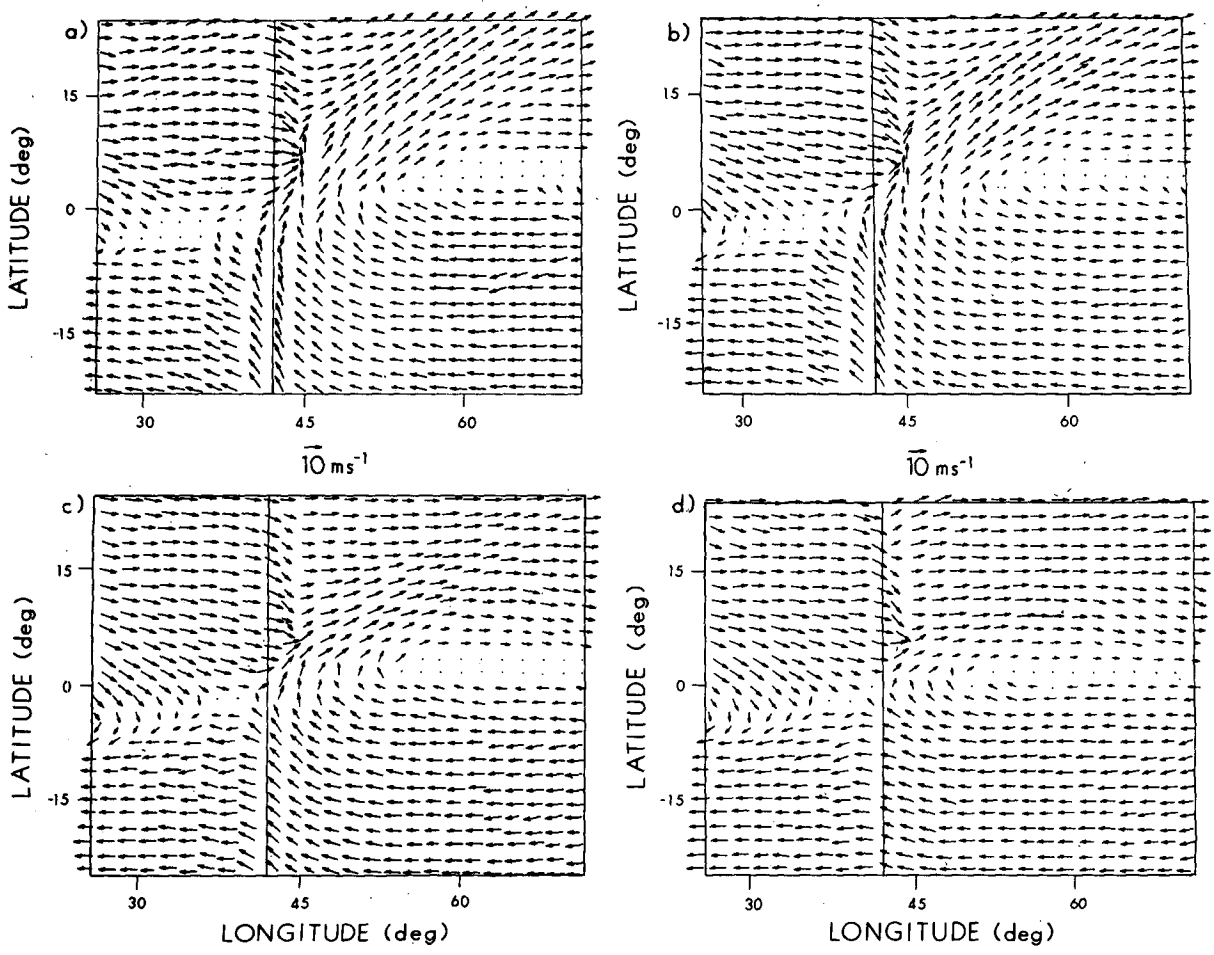

FIG. 3. The horizontal wind field at 72 h in the run with 1500 m topography to the west of a ledge at 42.187°E. Panels show wind vectors at vertical distances of (a) 119 m, (b) 529 m, (c) 1348 m and (d) 2168 m above the surface. To the east of the ledge, the surface is at sea level; to the west of the ledge, the surface is at 1500 m.

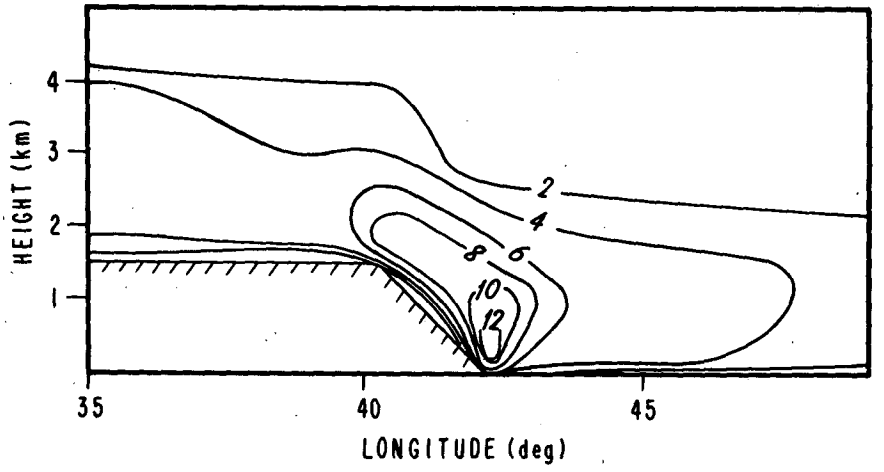

FIG. 4. Equatorial cross section of wind speed (contour interval 2 m s^{-1}) for the case shown in Fig. 3.

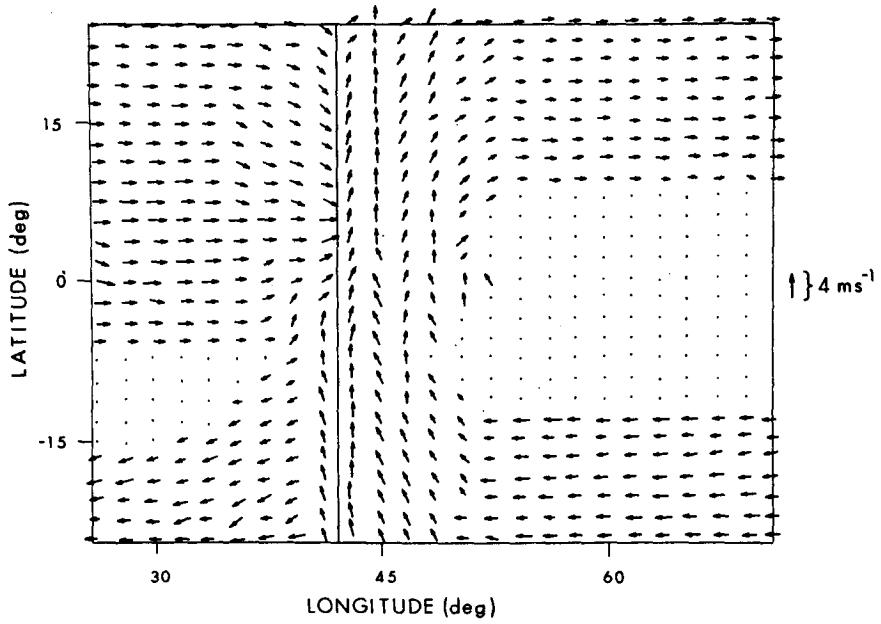

FIG. 5. The horizontal wind field at 72 h in the reduced forcing run with 1500 m topography to the west of a ledge at 42.187°E. The level is 529 m above the surface. The forcing is a factor of 10 smaller than that for the case shown in Fig. 3.

m above the surface in the case where the ledge is 3 km high. This is to be compared with Fig. 7b, which shows the flow at the same level in the case where the ledge is only 1 km high. We have done a mass balance calculation for both cases at this (529 m) level, which is essentially the level of the jet maximum. In the 3-km ledge case, all of the mass flux into the Southern Hemisphere moves northward across the equator in the region east of the ledge. In the 1-km ledge case, the corresponding figure is 45%. The remaining 55% moves upward and westward over the ledge.

c. *Realistic topography*

The East African topography we adopt for this run is that used in the operational forecast model at the ECMWF. This was obtained from archives at NCAR and is shown in Fig. 1. Peaks somewhat in excess of 2 km are resolved in East Africa and the island of Madagascar is represented. We have run the full model, all physics and the diurnal cycle included, with this topography present. Transient features are more persistent in this case compared to the cases just described

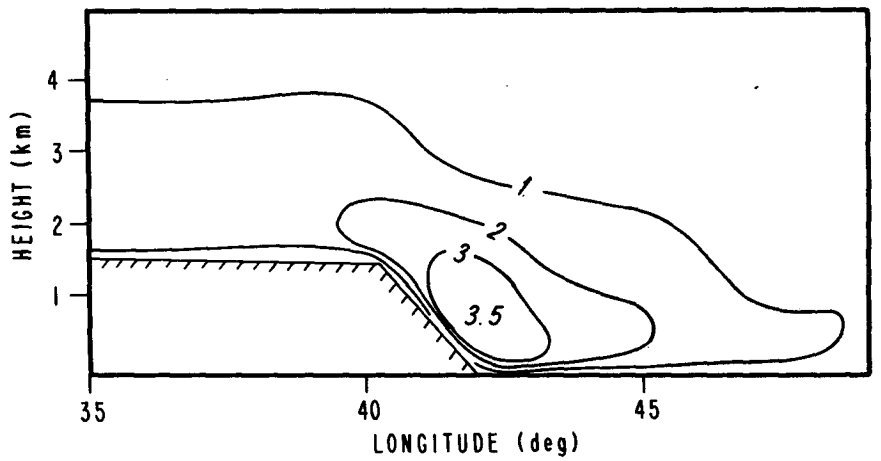

FIG. 6. Equatorial cross section of wind speed (contour interval 1 m s^{-1}) for the case shown in Fig. 5.

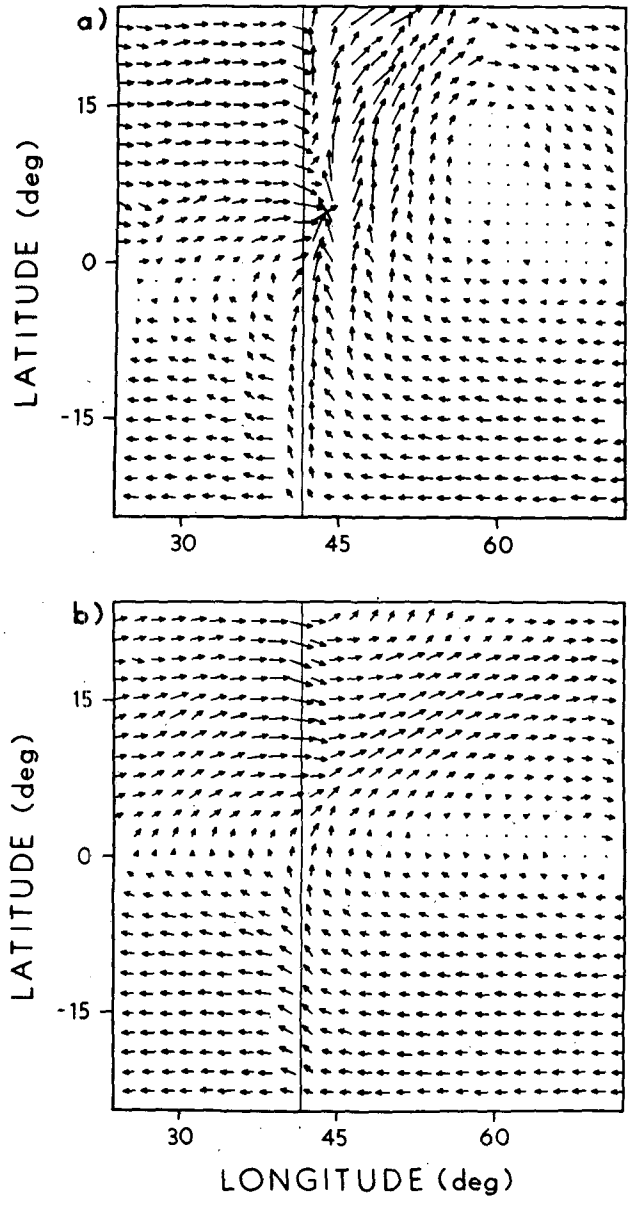

FIG. 7. The horizontal wind field at 529 m above the surface at 72 h in (a) the case with a 3-km high ledge and (b) the case with a 1-km high ledge. The forcing has the same amplitude as that for the case that was shown in Fig. 3.

with ledge topography and no model physics. It was necessary to run the model out beyond 7 days before the diurnal cycle became the only significant feature varying with time.

As in the idealized-topography runs, the forcing for this case is the zonally symmetric pressure distribution at the upper boundary that maintains the zonal wind given by (1). The response is illustrated in Fig. 8, which shows the 24-h average horizontal motion field 529 m above the terrain at day 9 of the run. The gross features of the observed circulation are reproduced. Specifically, the topography deflects the incident easterly winds into a concentrated region of southeasterly flow across the equator. Strong southerly winds are found east of the highest topography, and these southerly winds feed into a southwest monsoon north and east of the Horn of Africa. The equatorial cross section of wind speed is shown in Fig. 9. There is a well-defined jet, though as Fig. 8 shows, the wind direction in the jet is from the southeast rather than (as observed) the south. The jet maximum is located about 500 m above the local terrain near longitude 36°E, where the elevation is about 800 m.

d. Diurnal variation

In this subsection we analyze the diurnal variation of the response whose time-average pattern has just been discussed. The diurnal variation is essentially confined to the area over land and is largest in the region near the Horn of Africa. We select as an observation point the grid point located at 7.5°N, 46.875°E. This is located close to Burao (9.2°N, 45.3°E), a station for which Ardanuy (1979) presents a detailed time evolution of the jet obtained from frequent pibal ascents during the last week of June 1977.

Figure 10 shows two hodographs. The one in the upper left of the figure is obtained from the model; it shows the local-time diurnal variation of the wind 529 m above the surface from days 6 to 9. The hodograph in the right-hand part of the figure shows the observed local-time diurnal variation at 500 m above the station near Burao. This hodograph was constructed from the figures in Ardanuy (1979) showing the diurnal variation of the u and v components of the wind. The model diurnal variation and the observed diurnal variation agree in two respects: in both cases the wind speed is greater during the night, and in both cases the wind rotates anticlockwise during the period 0600 to 1800 and clockwise during the period 1800 to 0600. The principal difference between the two cases is that the diurnal-average wind in the model is from slightly east of south, while the observed diurnal-average wind is from the southwest.

The vertical distribution of the diurnal variation in the model is illustrated by Fig. 11. Here we show contours of the wind-speed anomaly relative to the diurnal-average wind speed and use a logarithmic scale for altitude. It can be seen that the main diurnal oscillation occurs in the layer between 100 and 1500 m, with a secondary oscillation appearing in the lowest 100 m. We have carried out two additional model experiments designed to establish the cause of the main diurnal oscillation. In the first of these we remove all topography from the model. In this experiment the diurnal-average wind is similar to that shown in Fig. 2; that is, it consists of zonal flow plus a small northward drift. Any diurnal variation of wind speed in this experiment could only be caused by the diurnal cycle of turbulent mixing or

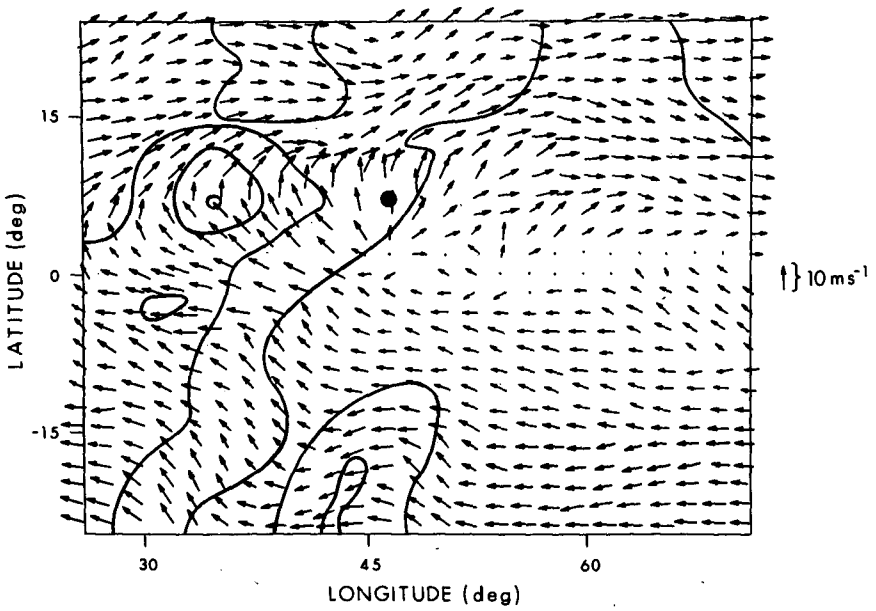

FIG. 8. The diurnal-average horizontal wind field at day 9 in the realistic topography run. The level is 529 m above the surface. Topography contours at an interval of 800 m have been included for reference.

possibly by a sea-breeze cycle. The diurnal variation of wind speed at the observation point (7.5°N, 46.875°E) is shown for this experiment in Fig. 12. The feature referred to in Fig. 11 as the main diurnal oscillation is absent. In the second experiment, topography is included, but we set to zero the prescribed zonal pressure distribution at the upper boundary which constitutes the external forcing in the model. In this experiment there is no forcing to drive flow over topography, and any diurnal variation of wind speed must then be a result only of buoyancy forces arising from the diurnal cycle of heating and cooling in the presence of sloping topography or possibly as a result of a sea-breeze cycle. The diurnal variation of wind speed at the observation point in this experiment is shown in Fig. 13. Absent again is the feature referred to in Fig. 10 as the main diurnal oscillation.

To summarize the results of these experiments: diurnal variation of vertical eddy diffusion and local phenomena such as a cycle of drainage winds or a sea breeze have little effect on the main diurnal oscillation. With the elimination of these possibilities there remains only one mechanism in the model to produce the main diurnal oscillation, and that is a tendency for the flow to go *over* the high topography of East Africa during the day and *around* (or along) the topography during the night. In this particular example, for which the observation point is 7.5°N, 46.875°E, the relevant high

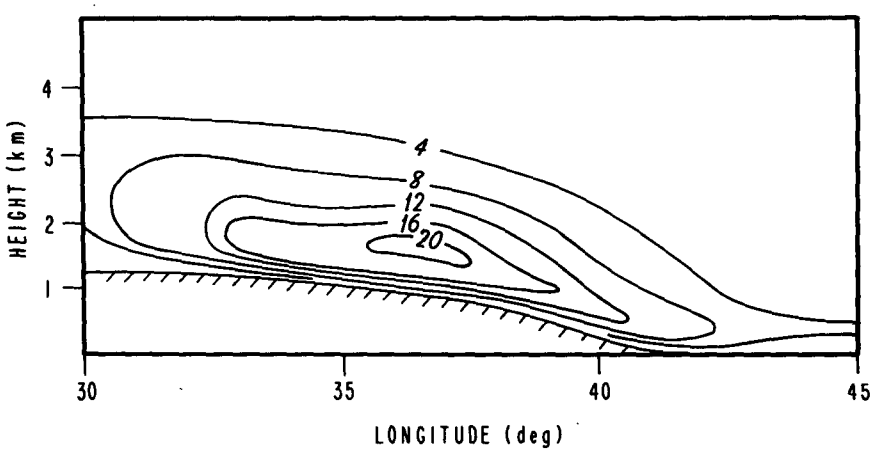

FIG. 9. Equatorial cross section of wind speed (contour interval 2 m s^{-1}) for the realistic-topography case shown in Fig. 8.

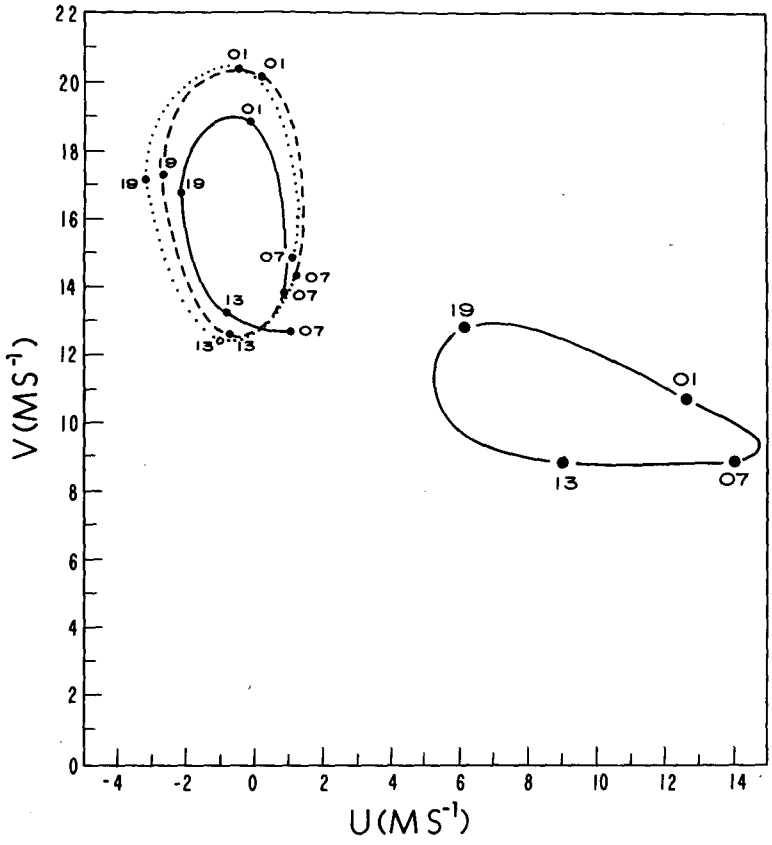

FIG. 10. Hodograph of wind speed at the observation point (7.5°N, 46.875°E) for days 6 through 9 in the realistic topography run shown at left. The height is 529 m above the terrain. Time is local time, with 6 h intervals denoted by filled circles on the respective days. Days 7, 8 and 9 are indicated by lines which are, respectively, solid, broken, and dotted. At right is shown a hodograph illustrating the observed diurnal variation of the wind at the 500-m level.

topography is probably the ridge located immediately west of the observation point (cf. Fig. 1). In order for this mechanism to operate, there must exist in the model a diurnal variation of static stability at low levels, with maximum static stability occurring during the nighttime hours. The existence of this is demonstrated by Fig. 14, which shows the diurnal variation of N^2 in the model calculated for the lowest kilometer above the ground at the observation point.

4. Discussion and conclusions

We have simulated some idealized versions of the EAJ using a planetary boundary layer model driven by zonally symmetric forcing applied at the model's upper boundary. The model was formulated in terrain-following coordinates and consisted of a stratified fluid of constant thickness. A possible solution for the combination of zonally symmetric forcing and a meridional topographic obstruction is zonally symmetric flow over the obstruction. Such a solution was not obtained in this investigation for the case of a meridional ledge or for the case of realistic East African topography. We conclude that the characteristic stratification of the model ($N^2 \approx 10^{-4}$ s^{-2}) and the finite height of East African topography (<2 km) is sufficient to divert a substantial fraction of the mass flux in the impinging Southern Hemisphere easterlies northward across the equator and into a flow that resembles the southwest monsoon. This conclusion could not be drawn from the several previous model studies in which *all* of the flow was forced northward across the equator by a western boundary filling the vertical domain occupied by the fluid. Even in the studies using models with topography of vertical extent less than fluid depth (Bannon, 1982; Krishnamurti et al., 1983), some of the northward flow is a response to the longitudinal dependence of the prescribed forcing.

The response to zonally symmetric forcing in the presence of straight-ledge topography exhibited several of the basic features seen in the observed flow pattern, including a region of southeast trades, a cross-equatorial jet, and a well-defined southwest monsoon. When the run was repeated with small-amplitude forcing (imposed zonal wind at the upper boundary of about 1 m s^{-1}), these features disappeared and were replaced by

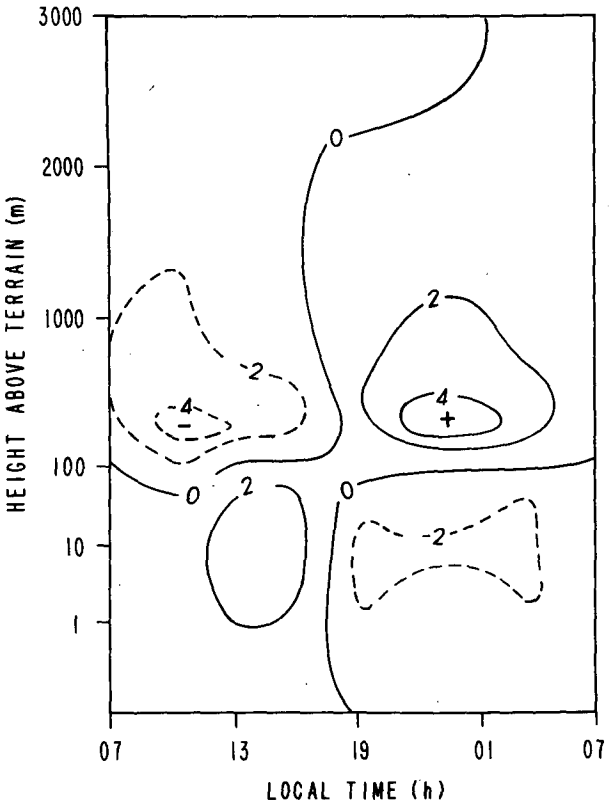

FIG. 11. Cross section at the observation point of the deviation of wind speed from the diurnal-average wind speed at day 9 in the realistic topography run. Contour interval is 2 m s^{-1}. Note that the altitude scale is logarithmic below 100 m.

a uniform flow northward along the ledge. The comparison of these two solutions illustrates that nonlinear dynamics provides the meridional asymmetry with respect to the equator that characterizes the summer circulation over the western Indian Ocean, as previously found in the barotropic model studies of Anderson (1976) and Bannon (1982).

The basic features of southeast trades, a cross-equatorial jet, and southwest monsoon are also present in the run with realistic topography, but detailed agreement between the simulated features and the observed features is lacking. The observed EAJ is quite narrow and almost southerly when it crosses the equator. Thereafter, it runs parallel to the coast a relatively short distance inland before breaking away near the Horn of Africa and intensifying to form the southwest monsoon. The model EAJ (Fig. 8) consists of a rather broad southeasterly flow across the equator that penetrates deep into the African highlands before recurving into a southwest monsoon. We attribute this feature of the response to the fact that the model forcing extends so far westward. Were the forcing confined to the Indian Ocean, as in EAJ models forced by a source–sink pair, instead of extending uniformly westward right across the African highlands, the blocking effect of the topography would certainly be felt farther eastward.

Although it is too far inland and has too much of an easterly component, the width of the model EAJ at the equator (Fig. 9) compares favorably with that of the EAJ at 2°S composited by Hart et al. (1978) from aircraft observations. The same observations show that the EAJ is already very concentrated as it passes north of Madagascar, with that island essentially blocking the flow and producing very large shear at its northern tip. The model EAJ (Fig. 8) does not possess this feature, the flow tending to pass over the island. It is likely that this also is an artifact of the forcing, which extends uniformly across the island.

The model exhibited a diurnal wind oscillation in the lowest 1500 m. At a chosen observation point inland from the Horn of Africa there was agreement of some features of the model oscillation and corresponding features of the oscillation observed by Ardanuy (1979): the wind backs during the day and veers during the night, and there is a nocturnal maximum in wind speed. Additional model runs were made with the topography removed and with the pressure gradient at the top of the model set to zero. On the basis of these experiments, we concluded that the mechanism producing the model diurnal wind oscillation in this region of East Africa is the modulation by diurnally varying static stability of the flow over topography. Specifically, when the static stability is low during daytime hours, the flow tends to go over the high topography west of

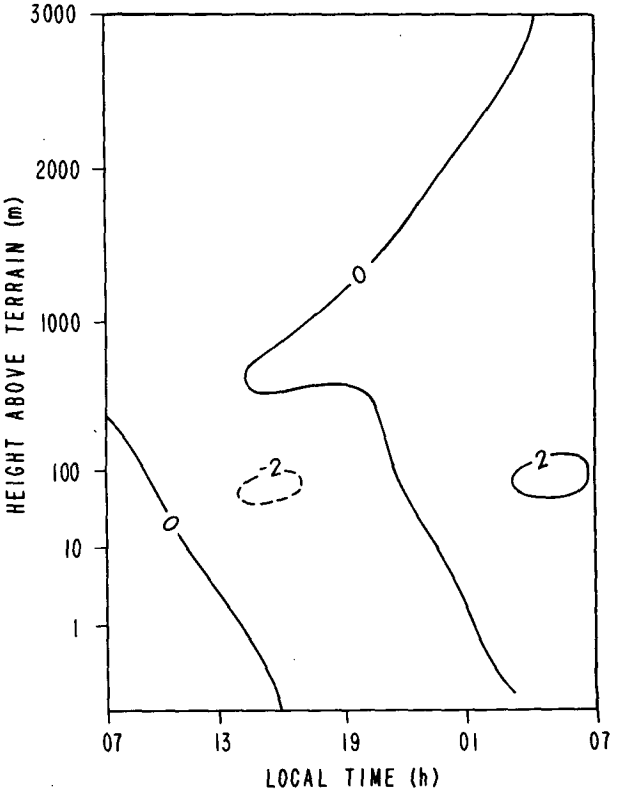

FIG. 12. As in Fig. 11, but for the run with all topography removed.

the observation point (denoted by a filled circle in Fig. 1). As illustrated by the hodograph of model wind (Fig. 10, left), the southerly wind present at the beginning of the day backs to come from a more southeasterly direction as the day progresses. During the nighttime hours the converse situation prevails, the wind veering back to southerly as the static stability increases.

Ardanuy (1979) was of the opinion that the most likely mechanism operating to produce the observed diurnal oscillation in wind speed was modulation by static stability through vertical eddy transport of momentum. Bannon (1979a) obtained a diurnal oscillation of 1.5 m s^{-1} amplitude at the equator in his barotropic-model EAJ when he parameterized the effect of vertical diffusion by Rayleigh friction having a 50% diurnal variation. Rubenstein (1981) developed a model which realistically treats vertical mixing, but confined his analysis to the development over a 6 h period of a daytime mixed layer in the EAJ well upstream of Ardanuy's observation point. Neither of these two model studies seems suitable for testing Ardanuy's hypothesis. The results presented here, derived from a model which contains a full diurnal cycle in the boundary layer, suggests that diurnal variation of static stability in conjunction with sloping topography is a more important mechanism than diurnal variation of vertical eddy transport in producing the low-level wind oscillation observed by Ardanuy (1979).

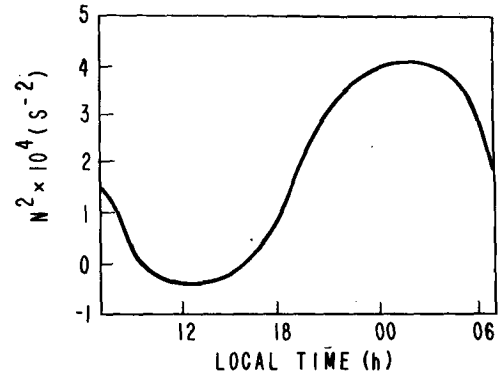

FIG. 14. The temporal behavior of low-level N^2 at the observation point at day 9 in the realistic topography run. Here N^2 is defined as $(g/\theta_0)(\theta_1 - \theta_0)/\Delta z$, where θ_1 is potential temperature at 1000 m, θ_0 potential temperature at 100 m above the surface, and Δz = 900 m.

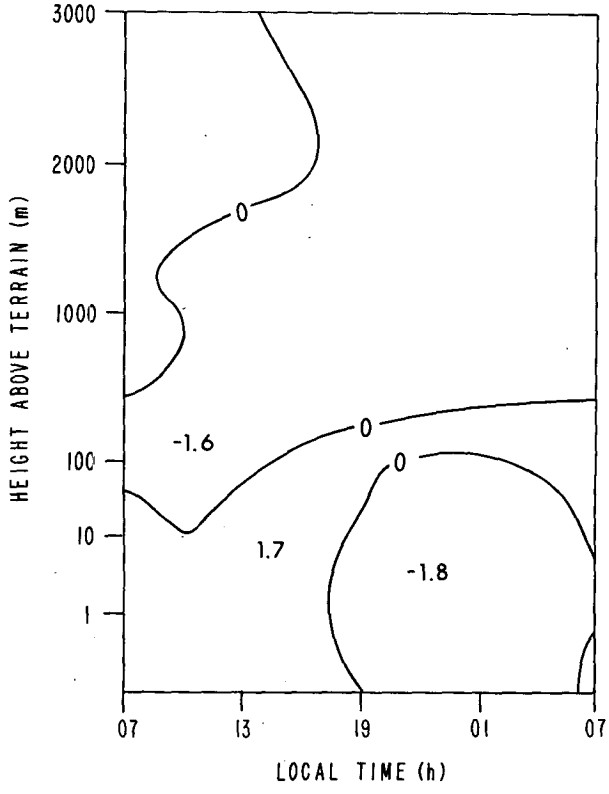

FIG. 13. As in Fig. 11, but for the run with upper boundary forcing set to zero.

Acknowledgments. The authors were supported by the National Science Foundation under Grants ATM-8121664 and ATM-8412272 (in the case of JP) and under Grants ATM-8120319 and ATM-8412687 (in the case of JEG). Computing resources were provided by the National Center for Atmospheric Research, which is sponsored by the National Science Foundation.

REFERENCES

Anderson, D. L. T., 1976: The low-level jet as a western boundary current. *Mon. Wea. Rev.*, **104,** 907–921.

Ardanuy, P., 1979: On the observed diurnal oscillation of the Somali jet. *Mon. Wea. Rev.*, **107,** 1694–1700.

Bannon, P. R., 1979a: On the dynamics of the East African jet. Part I. Simulation of mean conditions for July. *J. Atmos. Sci.*, **36,** 2139–2152.

——, 1979b: On the dynamics of the East African jet. Part II. Jet transients. *J. Atmos. Sci.*, **36,** 2153–2168.

——, 1982: On the dynamics of the East African jet. Part III. The Arabian Sea branch. *J. Atmos. Sci.*, **39,** 2267–2278.

Hart, J. E., 1977: On the theory of the East African low level jet stream. *Pure Appl. Geophys.*, **115,** 1263–1282.

——, G. V. Rao, H. van de Boogaard, J. A. Young and J. Findlater, 1978: Aerial observations of the East African low level jet stream. *Mon. Wea. Rev.*, **106,** 1714–1724.

Krishnamurti, T. N., J. Molinari and H. L. Pan, 1976: Numerical simulation of the Somali Jet. *J. Atmos. Sci.*, **33,** 2350–2362.

——, V. Wong, H. L. Pan, R. Pasch, J. Molinari and P. Ardanuy, 1983: A three-dimensional planetary boundary layer model for the Somali Jet. *J. Atmos. Sci.*, **40,** 894–908.

Paegle, J., and D. W. McLawhorn, 1983: Numerical modeling of diurnal convergence oscillations above sloping terrain. *Mon. Wea. Rev.*, **111,** 67–85.

Rubenstein, D. M., 1981: The daytime evolution of the East African Jet. *J. Atmos. Sci.*, **38,** 114–128.

Smagorinsky, J., 1963: General circulation experiments with the primitive equations. I. The basic experiment. *Mon. Wea. Rev.*, **91,** 99–164.

Zdunkowski, W. G., R. M. Welch and J. Paegle, 1976: One-dimensional numerical simulation of the effects of air pollution on the planetary boundary layer. *J. Atmos. Sci.*, **33,** 2399–2414.